A Tb/s Indoor Optical Wireless Access System Using VCSEL Arrays

Elham Sarbazi, Hossein Kazemi, Mohammad Dehghani Soltani, Majid Safari and Harald Haas

LiFi Research and Development Center, Institute for Digital Communications, School of Engineering,
University of Edinburgh, King's Buildings, Edinburgh, EH9 3FD, UK.
Email: {e.sarbazi, h.kazemi, m.dehghani, majid.safari, h.haas}@ed.ac.uk

Abstract—This paper presents a proof-of-concept for Tb/s infrared (IR) indoor optical wireless networks. We introduce a novel double tier access point architecture based on *array of arrays* of vertical cavity surface emitting lasers (VCSELs) to deliver beyond Tb/s aggregate capacity. For a given indoor environment, the optimal access point architecture is designed. The downlink performance is analysed throughout the coverage area and the spatial distribution of signal-to-interference-plus-noise ratio (SINR) and data rate are obtained. Numerical results demonstrate that with a single access point in a 25 m^2 indoor area, data rates of at least 10 Gb/s per beam are achieved almost everywhere and the aggregate data rate can exceed 2 Tb/s.

Index Terms—Optical wireless communication, 6G, indoor Tb/s access, VCSEL.

I. INTRODUCTION

In the past two decades, we have witnessed a rapid evolution of wireless communications. Nowadays, WiFi, 4th generation (4G) and 5th generation (5G) technologies are the main providers of high speed wireless data services. Mobile data traffic has globally grown 18 folds over the past five years and this trend is expected to continue in the coming years [1]. However, the ever-increasing demand for mobile capacity is indeed beyond the radio frequency (RF) spectrum capacity.

As a promising solution, optical wireless communication (OWC) opens a new spectrum, which is 2600 times the RF spectrum. OWC technology has been applied in both long range outdoor and space applications [2] and also short range indoor and personal area applications [3]. OWC exploits both the visible light spectrum and infrared (IR) spectrum. Visible light communication (VLC) refers to the data transfer between two single points using visible light. The bidirectional multi-user and fully networked variance of VLC is known as light fidelity (LiFi). Meanwhile, IR OWC provides a solution to the light dimming and the uplink glare problems associated with VLC, thereby supporting bidirectional communications [3].

Most OWC systems utilize light-emitting diodes (LEDs) as light sources, but LEDs suffer from poor electrical-to-optical conversion efficiency, limited bandwidth and broad spectral width, which makes narrow-band optical filtering less effective at the receiver. In this respect, the use of laser diodes (LDs) as light sources for high speed OWC systems can be more advantageous. Particularly, vertical cavity surface emitting lasers (VCSELs) have high modulation bandwidths well beyond 1 GHz, high efficiency and well-controlled

output beam properties. Compared to edge emitting lasers, VCSELs are easier to fabricate in arrays. The inherent low manufacturing cost, enhanced reliability, nonastigmatic and circularly symmetric optical output are other advantages of VCSELs over traditional edge emitting lasers [4].

OWC technology based on narrow-beam IR lasers has the potential to provide very high transmission rates for indoor multi-user wireless networks [5]–[8]. The beam-steered IR OWC systems can reach multi-Gb/s data rates over the confined spot of each beam by achieving a higher light intensity at the user's device and by utilizing the large modulation bandwidth of IR laser diodes. Targeting bit rates of up to 12.5 Gb/s for a single beam in [5], Wang *et al.* experimentally demonstrated an indoor point-to-point OWC system in which an optical fiber link is used to remotely guide the beam through free space using a lens and steering mirrors. Later in [6], they designed a photonic phased array integrated circuit to perform the same beam steering without mechanical mirrors. In [7], Koonen *et al.* proposed a wavelength-dependent diffractive system for two dimensional (2D) steering of multiple beams in free space from the same aperture by means of a fiber cable, a lens and cross-coupled Bragg gratings. The steering of each beam is remotely controlled by adjusting the wavelength of the light fed into the fiber link using tunable laser diodes, achieving a net data rate of 32 Gb/s per IR beam in the downlink. In [8], the authors implemented wavelength-controlled beam steering for a large number of beams based on a passive optical module called high port count arrayed waveguide grating router (AWGR), which is coupled to a 2D fiber array to orient different beams in the desired directions with a lens. They reported transmissions at a peak data rate of 112 Gb/s using 4-pulse amplitude modulation (PAM) and concluded that a system throughput of 8.9 Tb/s can be achieved by an 80-port AWGR.

The aforementioned works apply advanced optical designs for beam steering to provide IR laser beam-class indoor coverage. The high complexity and expensive components of such designs may not suit large-scale deployments in indoor networks. Aiming for ultra-high transmission capacities, in this work, we consider IR VCSEL-based OWC systems for indoor applications. We propose a novel double tier access point (AP) architecture based on an array of VCSEL arrays, which is also referred to as the *array of arrays* for brevity. In this architecture, each array is oriented in a specific direction
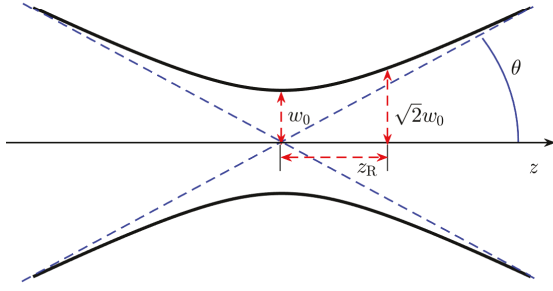
Fig. 1. Gaussian beam parameters.

to cover a certain area of the floor where data rates of at least 10 Gb/s per beam can be realized using direct current-biased optical orthogonal frequency division multiplexing (DCO-OFDM), leading to aggregate data rates greater than 2 Tb/s from a single AP. The proposed design is elaborated in terms of the received SINR and transmission rate per beam.

The remainder of this paper is organized as follows. In Section II, the characteristics of Gaussian beams are discussed. In Section III, the double tier access point architecture is introduced and the overall system model is presented. In Section IV, the link performance is evaluated. Section V provides some numerical results and relevant discussions. Finally, concluding remarks are provided in Section VI.

II. GAUSSIAN BEAM PROPAGATION

In most applications, the laser beam is assumed to have a Gaussian intensity profile. A Gaussian beam is characterized by two parameters: beam waist w_0 and wavelength λ. The beam waist is where the wavefront is planar and the beam diameter is minimum. It can be either real or, more commonly, virtual (i.e., by projecting backward inside the laser). Assuming that the beam is travelling along the z axis and the beam waist is located at the origin of cylindrical coordinates, the intensity distribution is given by [9]:

$$I(r,z) = \frac{2P_\mathrm{t}}{\pi w^2(z)} \exp\left(-\frac{2r^2}{w^2(z)}\right), \qquad (1)$$

where P_t is the optical power carried by the beam, and r and z are the radial and axial positions, respectively. The beam radius $w(z)$ is expressed as [9]:

$$w(z) = w_0 \sqrt{1 + \left(\frac{z}{z_\mathrm{R}}\right)^2}. \qquad (2)$$

The Rayleigh range z_R is given by:

$$z_\mathrm{R} = \frac{\pi w_0^2 n}{\lambda}, \qquad (3)$$

where n represents the refractive index of the medium [9].

A qualitative picture of a Gaussian beam and its main parameters are shown in Fig. 1. Although the tail of the Gaussian beam intensity never actually reaches zero, the *edge* of the beam is considered to be the radial distance $r = w(z)$. That is where the intensity drops to $\exp(-2)$ of its value on axis. The divergence angle of the beam is defined as [9]:

$$\theta = \lim_{z \to \infty} \arctan\left(\frac{w(z)}{z}\right) \simeq \frac{\lambda}{\pi w_0 n}. \qquad (4)$$

Also, the complex q-parameter of the beam which is often used in simplified Gaussian beam field equations, is defined as the following expression [9]:

$$q(z) = z + j z_\mathrm{R} \qquad (5)$$

A Gaussian beam can be fully characterized by its q-parameter. Other than this, w_0 and λ can determine all the beam properties.

A. Beam Transformation By Lens

When refracted by a lens, a Gaussian beam is transformed into another Gaussian beam characterized by a different set of parameters. A method to relate the input and output of any optical system is the use of ray transfer or ABCD matrices [9], where a 2×2 matrix relates the position and angle of paraxial rays at the input and output planes of the optical system through linear algebraic equations. For Gaussian beams, however, the ABCD law is applied to the q-parameters [9]. In the following, this method is briefly explained.

Let the input and output beam waists be regarded as the object and the image, respectively. Depending on the lens type and location of the beam with respect to the lens, either the object and the image may be real or virtual. Let w_0, z_R and q be the corresponding parameters of the input Gaussian beam, and let w_0', z_R' and q' be those of the output Gaussian beam. The complex beam parameters q and q' are related by [9]:

$$q' = \frac{Aq + B}{Cq + D}, \qquad (6)$$

with the matrix elements [10]:

$$A = 1 + \frac{d(n-1)}{n\rho_1} \qquad (7a)$$

$$B = \frac{d}{n} \qquad (7b)$$

$$C = (n-1)\left(\frac{1}{\rho_1} - \frac{1}{\rho_2}\right) - \frac{d(n-1)^2}{n\rho_1\rho_2} \qquad (7c)$$

$$D = 1 - \frac{d(n-1)}{n\rho_2} \qquad (7d)$$

where d represents the lens thickness and n is the refractive index of the lens. Also, ρ_1 and ρ_2 are the radii of the input and output surfaces of the lens, respectively. The knowledge of the complex parameter q' is sufficient to determine the characteristics of the output beam.

III. DOUBLE TIER ACCESS POINT ARCHITECTURE

A. Array of Arrays Model

The proposed double tier AP architecture based on the array of arrays model is depicted in Fig. 2. Let N_VCSEL denote the total number of VCSELs in the double tier AP. In the example design as shown in Fig. 2, there are nine 5×5 VCSEL arrays, leading to $N_\mathrm{VCSEL} = 225$. In this paper, we assume that the optical beam of each VCSEL is assigned to a single user. The AP employs a two tier transmission protocol for the downlink connection per beam in order to transmit by the right beam to the desired user. First, the array that accommodates the user's
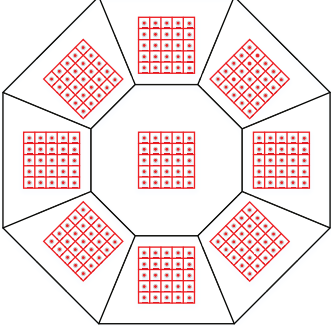
2

Fig. 2. Double-tier access point architecture using array of arrays of VCSELs (top view). This design involves nine 5×5 VCSEL arrays.

spot is determined. Then, from that array, the VCSEL covering the user's spot is identified.

B. Optical OFDM

An effective approach to achieve high data rates in OWC systems relies on optical OFDM techniques. A widely adopted and the most bandwidth efficient variant of optical OFDM is DCO-OFDM, in which the varying envelope of the time domain signal is shifted to a positive level using a DC bias to fulfil the non-negativity constraint of intensity modulation and direct detection (IM-DD) channels [11]. Following a digital realization of DCO-OFDM based on N-point inverse fast Fourier transform (IFFT) and fast Fourier transform (FFT) operations at the transmitter and receiver, respectively, data symbols are modulated per subcarrier using quadrature amplitude modulation (QAM), then they are loaded onto $N-2$ data-carrying subcarriers. To ensure a purely real-valued time domain signal, Hermitian symmetry is enforced on the OFDM frame before applying the N-IFFT.

Assume that each VCSEL is individually driven by a DCO-OFDM waveform to transmit an independent data stream exclusively intended for the user within its coverage spot. The instantaneous optical power emitted by the ith VCSEL at time sample t, for $t = 0, 1, \ldots, N - 1$ is given by:

$$x_i(t) = \sqrt{P_i} s_i(t) + x_{\mathrm{DC}}, \qquad (8)$$

where P_i is the average electrical power of the OFDM symbol; $s_i(t)$ is the normalized discrete time OFDM signal; and x_{DC} is the DC bias, which is equal to the average optical power denoted by P_{t}.

The envelope of the OFDM signal before biasing follows a zero mean real Gaussian distribution for $N \geq 64$ [12]. Therefore, the instantaneous optical power in (8) randomly varies around x_{DC} with a variance of P_i. The value of the DC bias is chosen such that the finite dynamic range of the VCSEL can accommodate the peak-to-peak variations of $x_i(t)$ while minimal clipping is caused. A practical design criterion is to use $x_{\mathrm{DC}} = 3\sqrt{P_i}$, to make sure that in 99.7% of time $x_i(t)$ varies within three standard deviations of the Gaussian distribution, i.e., within $(-x_{\mathrm{DC}}, +x_{\mathrm{DC}})$. This guarantees that 99.7% of the signal envelope is undistorted,

and the clipping noise is negligible [13]. Therefore, the average electrical power for VCSEL$_i$ is obtained as $P_i = \frac{1}{9}P_{\mathrm{t}}^2$ for $i = 1, 2, \ldots, N_{\mathrm{VCSEL}}$.

Assuming that the user's receiver is associated with VCSEL$_i$, the received photocurrent is:

$$y(t) = R_{\mathrm{PD}} h_i x_i(t) + \sum_{j \neq i} R_{\mathrm{PD}} h_j x_j(t) + v(t), \qquad (9)$$

where R_{PD} is the photodiode (PD) responsivity and h_j denotes the DC gain of the channel between the jth VCSEL located at (a_j, b_j) and the PD at the receiver and is given by:

$$h_j = \iint\limits_{\mathcal{A}_{\mathrm{PD}}} \frac{2}{\pi w^2(z)} \exp\left(-2\frac{(x - a_j)^2 + (y - b_j)^2}{w^2(z)}\right) dxdy, \qquad (10)$$

where $\mathcal{A}_{\mathrm{PD}}$ denotes the set of points on the x-y plane with the desired PD located at the origin, covering the whole area of the PD. Here, $|\mathcal{A}_{\mathrm{PD}}| = A_{\mathrm{PD}}$ where $|\cdot|$ denotes the cardinality of a set and A_{PD} is the PD area. In (9), $v(t)$ is an additive white Gaussian noise (AWGN), composed of thermal noise, shot noise of the receiver, and the relative intensity noise (RIN) of the VCSELs. The total noise variance is given by (11) at the top of the next page, where k is the Boltzmann constant; T is temperature in Kelvin; R_{L} is the load resistance; B is the single-sided bandwidth of the system; F_{n} is the noise figure of the transimpedance amplifier (TIA); q_{e} is the elementary charge; and RIN is the power spectral density (PSD) of the laser noise, defined as the mean square of intensity fluctuations of the laser source normalized to the squared average intensity [14].

C. Eye Safety Considerations

In practice, the maximum optical power emitted from a VCSEL is subject to eye safety regulations. As such, the so-called maximum permissible exposure (MPE) is introduced in the laser safety standards which specifies the maximum irradiance of the laser source [15]. MPE depends on the source wavelength, angular subtense and exposure time. The angular subtense α is defined as the plane angle subtended by an apparent source as viewed from a point in space. According to [15], if at the given measurement distance $\alpha < 1.5$ mrad, the source is termed as a *point source*, otherwise an *extended source*.

A laser source is considered to be safe, if at any position in space, the fraction of the received power passing through the pupil of the human eye is less than the corresponding MPE value multiplied by the pupil area A_{pupil}. The laser safety analysis, therefore, often includes determining the most hazardous position (MHP), i.e., where the power received at the pupil aperture is at its maximum. If the eye safety condition is met at this point, it ascertains that anywhere else in space is also eye-safe [16].

In this work, the eye safety limits have been taken into account. The MHP is specified as 10 cm [16] and the maximum permissible optical power for each VCSEL is calculated as $P_{\mathrm{opt,max}} = 16$ mW which satisfies the eye safety condition.

$$\sigma^2 = \frac{4kT}{R_{\mathrm{L}}}BF_{\mathrm{n}} + 2q_{\mathrm{e}}\left(\sum_{j=1}^{N_{\mathrm{VCSEL}}} R_{\mathrm{PD}}h_j P_{\mathrm{t}}\right)B + \mathrm{RIN}\left(\sum_{j=1}^{N_{\mathrm{VCSEL}}}(R_{\mathrm{PD}}h_j P_{\mathrm{t}})^2\right)B \tag{11}$$

IV. DATA RATE ANALYSIS

A. Signal-to-Interference-plus-Noise Ratio

Assuming that all the AP VCSELs are active and serving a user, the SINR at the user's receiver from VCSEL$_i$ is derived using (9) as follows:

$$\gamma_i = \frac{R_{\mathrm{PD}}^2 h_i^2 P_i}{\sum_{j\neq i} R_{\mathrm{PD}}^2 h_j^2 P_j + \sigma^2}. \tag{12}$$

B. Data Rate per VCSEL

In this paper, the reliable transmission rate for each VCSEL is determined based on the bit error ratio (BER) performance. For the AWGN channel as described in Section III-B, the exact BER expression of M-ary square QAM is a summation of M terms [17]. A tight upper bound for the BER performance of the M-QAM OFDM-based OWC system, accurate to within 1 dB for $M \geq 4$ and $0 \leq \gamma_i \leq 30$ dB, is given by [17]:

$$\mathrm{BER} \leq 0.2\exp\left(-\frac{1.5\gamma_i}{M-1}\right), \tag{13}$$

where γ_i is given in (12). Let M_i denote the QAM size assigned to VCSEL$_i$. In order to maintain the same BER for all links, the highest order of the QAM constellation can be obtained by solving (13) with equality for M_i, which yields:

$$M_i = 1 + \frac{\gamma_i}{\Gamma}, \tag{14}$$

where:

$$\Gamma = \frac{-\ln(5\mathrm{BER})}{1.5}, \tag{15}$$

models the SINR gap due to the required BER performance, which is specified by the forward error correction (FEC) limit.

From (14), the number of transmitted bits per channel use for each subcarrier becomes $\log_2 M_i$. With an OFDM symbol rate of $\frac{2B}{N}$ symbol/s, the bit rate per subcarrier is given by $\frac{2B}{N}\log_2 M_i$ bits/s. According to $\frac{N}{2}-1$ data-carrying subcarriers in DCO-OFDM, the data rate for VCSEL$_i$ is of the form:

$$R_i = \xi B\log_2 M_i, \tag{16}$$

where $\xi = \frac{N-2}{N}$ is the subcarrier utilization factor.

V. RESULTS AND DISCUSSIONS

In each VCSEL array, the elements are placed very close to each other. As a result, their beam spots may significantly overlap at the receiver plane. In order to separate the beams, a lens can be employed in front of each array. The function of lens is to refract the output lights from different VCSELs towards different directions, providing high spatial resolutions. The refraction angle that each VCSEL experiences depends on the lens thickness and the path it takes within the lens. To

TABLE I
SIMULATION PARAMETERS

Parameter	Symbol	Value
Link distance	z	3 m
VCSEL wavelength	λ	950 nm
Beam waist	w_0	5 μm
VCSEL bandwidth	B	5 GHz
Laser noise PSD	RIN	-155 dB/Hz
Lens refractive index	n	1.5
PD area	A_{PD}	2 cm^2
Load resistance	R_{L}	50 Ω
TIA noise figure	F_{n}	5 dB
FEC limit	BER	10^{-3}

achieve the desired spatial separation of the beams, the lens dimensions need to be determined accordingly.

Consider a 5×5 array of VCSELs and a plano-convex lens at a 5 mm distance from the array. Let L, R and d_0 denote the edge diameter, the radius of curvature and the constant thickness of the lens. Figs. 3 and 4 illustrate the effect of these parameters on the beam separation. In these figures, the spatial distribution of the received light intensity on the floor is displayed by assuming $P_{\mathrm{t}} = 1$ mW. In Fig. 3, the lens is rather large ($L = 24$ mm). With $R = 25$ mm, a square beam spot with uniform intensity is formed. For $R = 17$ mm, the beams are still largely overlapping. By using $R = 15$ mm, the beams are sufficiently separated, although there is a slight overlap between the adjacent beam spots. In Fig. 4, the lens is smaller ($L = 16$ mm). It can be seen that by reducing the radius of curvature, the refraction angles increase and the beams move apart considerably.

Next, we present an example link design for a $5 \times 5 \times 3$ m^3 room. A double tier AP is mounted at the centre of the ceiling to cover the floor area of 25 m^2. The AP is equipped with 9 VCSEL arrays with each array consisting of 5×5 VCSEL elements, as shown in Fig. 2. So, each array is responsible for covering almost $1/9$ of the room area. The total area of each VCSEL array is assumed to be 1 cm^2 (i.e. with a 0.2 cm spacing between adjacent elements). Also, the VCSEL arrays are placed in a 2 cm distance from each other on the AP. The orientation of each VCSEL array is adjusted such that it covers a specific part of the floor plane. For example, the middle VCSEL array is not tilted and it covers an area of 1.5×1.5 m^2 at the centre of the floor. A suitable lens with the same tilt angle is also placed in front of each VCSEL array. The rest of the system parameters used for simulations are listed in Table I; VCSEL and noise parameters are adopted from [18]. In what follows, we consider three scenarios.
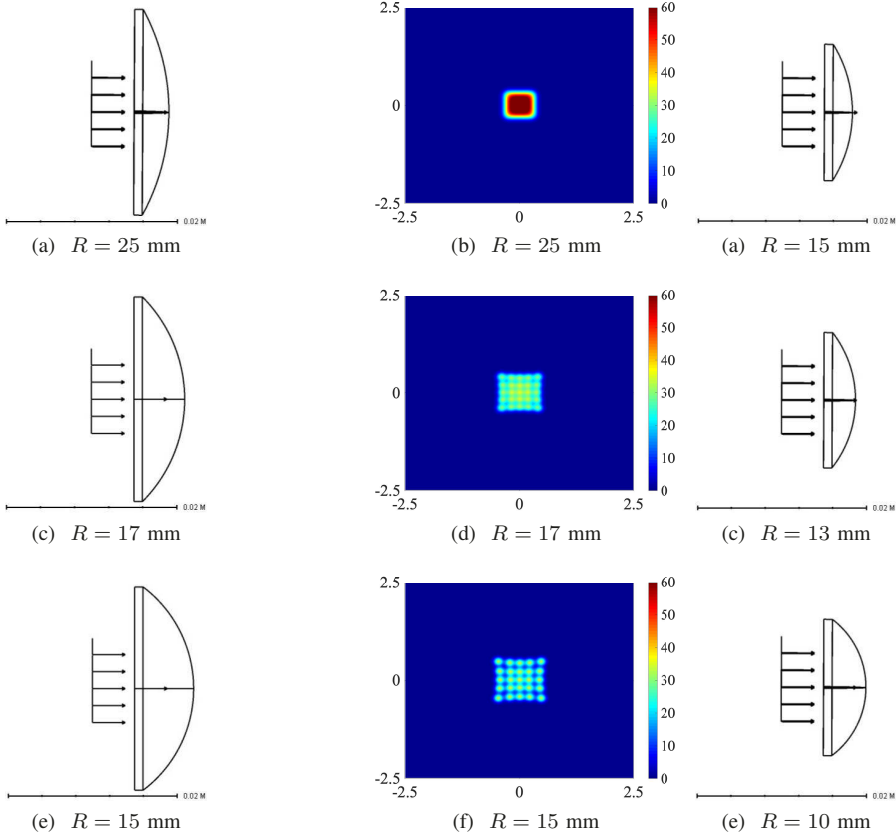
(a) $R = 25$ mm

(b) $R = 25$ mm

(c) $R = 17$ mm

(d) $R = 17$ mm

(e) $R = 15$ mm

(f) $R = 15$ mm

Fig. 3. Spatial distribution of normalized I at $z = 3$ m for different lenses ($L = 24$ mm).

(a) $R = 15$ mm

(b) $R = 15$ mm

(c) $R = 13$ mm

(d) $R = 13$ mm

(e) $R = 10$ mm

(f) $R = 10$ mm

Fig. 4. Spatial distribution of normalized I at $z = 3$ m for different lenses ($L = 16$ mm).

A. Scenario 1

In scenario 1, the output power of each VCSEL element is $P_t = 10$ mW, which is less than the maximum permissible value determined according to the laser safety regulations. Figs. 5(a) and 5(b), respectively, show the spatial distribution of the received SINR and that of the data rate on the floor. As seen in these figures, data rates of 15 to 20 Gb/s are achieved at the beam spot centres. Besides, a data rate of at least 10 Gb/s is guaranteed almost everywhere on the floor, except at the beam spot borders and in locations very close to the walls. Providing at least 10 Gb/s per beam, the AP delivers the aggregate data rate of beyond 225×10 Gb/s $= 2.25$ Tb/s.

B. Scenario 2

In scenario 2, all the VCSELs are assumed to transmit with an optical power of $P_t = 7$ mW. Figs. 6(a) and 6(b), respectively, show the received SINR and data rate distributions on the floor. In this case, data rates higher than 15 Gb/s are only achieved at the beam spot centres in locations close to the centre of the room. When moving away from the room centre, the data rate level experiences frequent ups and downs. Nonetheless, a data rate of 5 Gb/s is still ensured in most locations and the aggregate data rate is greater than 1 Tb/s.
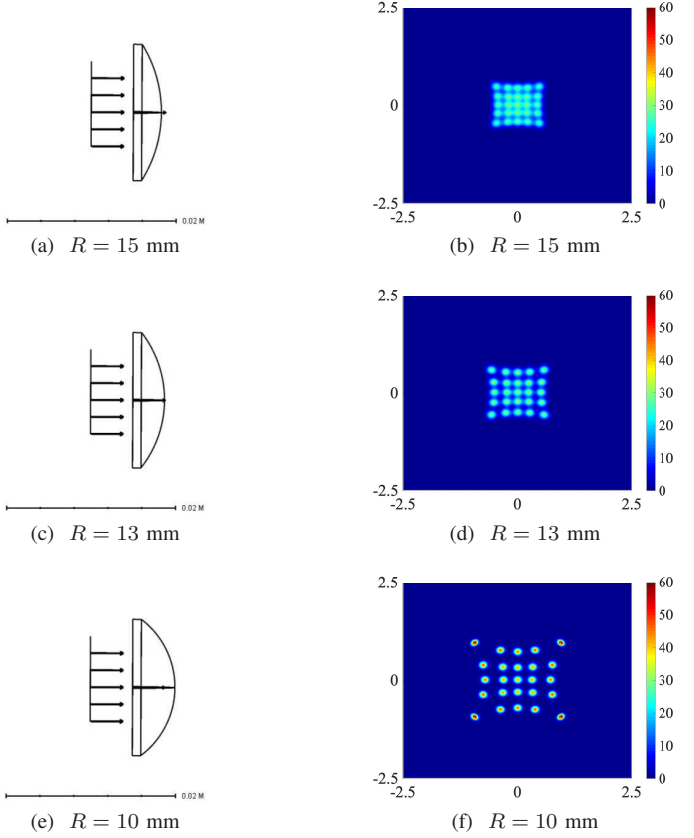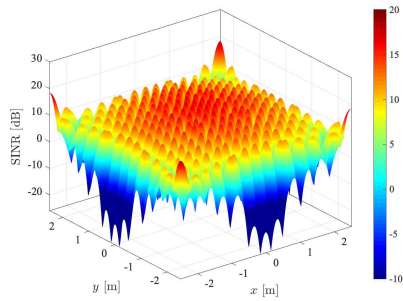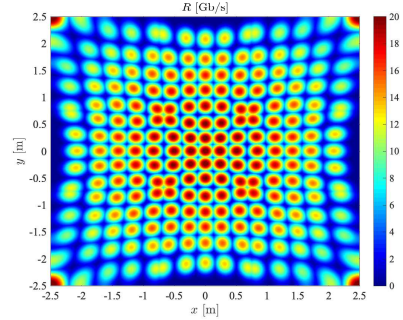
C. Scenario 3

Let the total area of the floor be divided into three zones, as illustrated below:

| 3	2	3
2	1	2
3	2	3

According to the simulation results of scenarios 1 and 2, zone 1 receives the highest average SINR level, while zone 3 receives the lowest. In scenario 3, the transmit power of the VCSELs are chosen such that the VCSEL array covering zone 1 has lower and those covering zone 3 have higher transmit power. We consider $P_t = 7$ mW, 8 mW and 10 mW for zones 1, 2 and 3, respectively. The spatial distributions of the received SINR and the data rate are plotted in Figs. 7(a) and 7(b). It can be observed that similar to scenario 1, data rates of at least 10 Gb/s are achieved almost everywhere. Comparing scenarios 1 and 3, it is evident that scenario 3 is more power efficient. In this case, similar to scenario 1, the aggregate data rate is beyond 2.25 Tb/s, while saving 3 mW per VCSEL for zone 1 and 2 mW per VCSEL for zone 2 relative to scenario 1. This zone-based power adaptation yields a total power saving of 275 mW (12.2% compared to scenario 1) for the double tier AP.
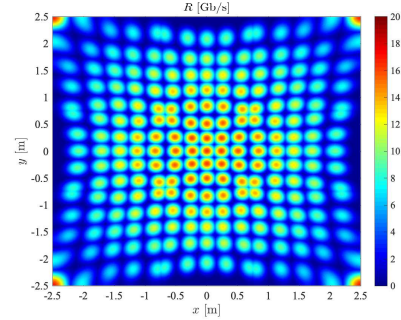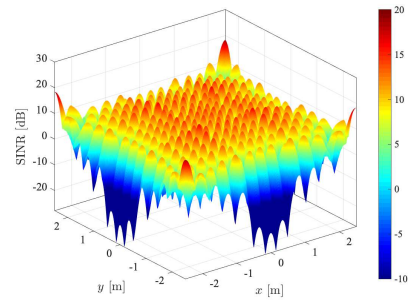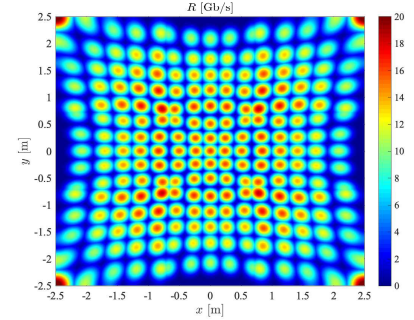
(a)
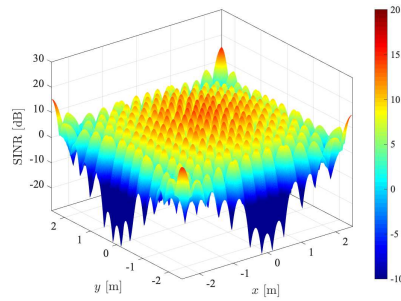
(b)

Fig. 5. Spatial distribution of SINR and data rate at $z = 3$ m for scenario 1 with $P_t = 10$ mW.

(a)

(b)

Fig. 6. Spatial distribution of SINR and data rate at $z = 3$ m for scenario 2 with $P_t = 7$ mW.

(a)

(b)

Fig. 7. Spatial distribution of SINR and data rate at $z = 3$ m for scenario 3 with $P_t = 7/8/10$ mW.

VI. CONCLUSION

We have exploited the potential of IR indoor optical wireless transmission for offering Tb/s aggregate capacities. A novel double tier access point architecture has been devised which consists of multiple narrow beam VCSEL arrays. By optimising the number and orientation of individual arrays, a full coverage with minimum beam spot overlaps has been achieved for a given indoor environment. This design provides a data rate of at least 10 Gb/s per beam and therefore leads to an aggregate data rate greater than 2 Tb/s. In future works, a multi-user system with reduced user and inter-cell interference will be developed. Also, the feasibility of beam steerable options for higher data rates will be considered.

ACKNOWLEDGMENT

REFERENCES

[1] Cisco, "Cisco Visual Networking Index: Global Mobile Data Traffic Forecast Update, 2017–2022," *White Paper*, 2019.

[2] V. W. Chan, "Free-Space Optical Communications," *IEEE/OSA J. Lightw. Technol.*, vol. 24, no. 12, pp. 4750–4762, Dec. 2006.

[3] H. Elgala, R. Mesleh, and H. Haas, "Indoor Optical Wireless Communication: Potential and State-of-the-Art," *IEEE Commun. Mag.*, vol. 49, no. 9, pp. 56–62, Sep. 2011.

[4] R. Michalzik, *VCSELs: Fundamentals, Technology and Applications of Vertical-Cavity Surface-Emitting Lasers*. Springer, 2012, vol. 166.

[5] K. Wang, Z. Yuan *et al.*, "Experimental Demonstration of Indoor Infrared Optical Wireless Communications with a Silicon Photonic Integrated Circuit," *IEEE J. Lightw. Technol.*, vol. 37, no. 2, pp. 619–626, 2018.

[6] K. Wang, A. Nirmalathas, C. Lim, and E. Skafidas, "High-Speed Optical Wireless Communication System for Indoor Applications," *IEEE Photon. Technol. Lett.*, vol. 23, no. 8, pp. 519–521, 2011.

[7] T. Koonen, J. Oh *et al.*, "Ultra-High Capacity Indoor Optical Wireless Communication Using 2D-Steered Pencil Beams," *IEEE/OSA J. Lightw. Technol.*, vol. 34, no. 20, pp. 4802–4809, 2016.

[8] T. Koonen, F. Gomez-Agis *et al.*, "High-Capacity Optical Wireless Communication Using Two-Dimensional IR Beam Steering," *IEEE/OSA J. Lightw. Technol.*, vol. 36, no. 19, pp. 4486–4493, 2018.

[9] B. E. A. Saleh and M. C. Teich, *Fundamentals of Photonics*, 3rd ed. John Wiley & Sons, Inc., 2019, vol. Part I: Optics.

[10] E. Hecht, "Optics," *Addison-Wesley*, pp. 384–441, 2002.

[11] O. Gonzalez, R. Perez-Jimenez *et al.*, "OFDM over indoor wireless optical channel," *IEEE Proceedings - Optoelectronics*, vol. 152, no. 4, pp. 199–204, Aug. 2005.

[12] D. Dardari, V. Tralli, and A. Vaccari, "A Theoretical Characterization of Nonlinear Distortion Effects in OFDM Systems," *IEEE Trans. Commun.*, vol. 48, no. 10, pp. 1755–1764, Oct. 2000.

[13] S. Dimitrov, S. Sinanovic, and H. Haas, "Clipping Noise in OFDM-Based Optical Wireless Communication Systems," *IEEE Trans. Commun.*, vol. 60, no. 4, pp. 1072–1081, Apr. 2012.

[14] L. A. Coldren, S. W. Corzine, and M. L. Masanovic, *Diode Lasers and Photonic Integrated Circuits*, 2nd ed. John Wiley & Sons, Inc., 2012.

[15] *Safety of Laser Products - Part 1: Equipment Classification, Requirements and User's Guide*, International Electrotechnical Commission (IEC) 60825-1:2014 Std., Aug. 2014.

[16] R. Henderson and K. Schulmeister, *Laser Safety*. CRC Press, 2003.

[17] A. J. Goldsmith and S.-G. Chua, "Variable-Rate Variable-Power MQAM for Fading Channels," *IEEE Trans. Commun.*, vol. 45, no. 10, pp. 1218–1230, Oct. 1997.

[18] K. Szczerba, P. Westbergh *et al.*, "4-PAM for High-Speed Short-Range Optical Communications," *IEEE/OSA J. Opt. Commun. Netw.*, vol. 4, no. 11, pp. 885–894, Nov. 2012.